

Magnetism and d-wave superconductivity on the half-filled square lattice with frustration

Andriy H. Nevidomskyy^{1,*}, Christian Scheiber², David Sénéchal¹, and A.-M. S. Tremblay¹

¹*Département de physique, Université de Sherbrooke, Sherbrooke, Québec, J1K 2R1, Canada*

²*Institute of Theoretical and Computational Physics,*

Graz University of Technology, Petersgasse 16, 8010 Graz, Austria

(Dated: February 9, 2022)

The role of frustration and interaction strength on the half-filled Hubbard model is studied on the square lattice with nearest and next-nearest neighbour hoppings t and t' using the Variational Cluster Approximation (VCA). At half-filling, we find two phases with long-range antiferromagnetic (AF) order: the usual Néel phase, stable at small frustration t'/t , and the so-called collinear (or super-antiferromagnet) phase with ordering wave-vector $(\pi, 0)$ or $(0, \pi)$, stable for large frustration. These are separated by a phase with no detectable long-range magnetic order. We also find the d-wave superconducting (SC) phase ($d_{x^2-y^2}$), which is favoured by frustration if it is not too large. Intriguingly, there is a broad region of coexistence where both AF and SC order parameters have non-zero values. In addition, the physics of the metal-insulator transition in the normal state is analyzed. The results obtained with the help of the VCA method are compared with the large- U expansion of the Hubbard model and known results for the frustrated J_1 - J_2 Heisenberg model. These results are relevant for pressure studies of undoped parents of the high-temperature superconductors: we predict that an insulator to d-wave SC transition may appear under pressure.

PACS numbers: 71.10.Fd, 74.72.-h, 71.30.+h, 75.10.Jm

I. INTRODUCTION

The subject of frustration¹ in quantum magnetic systems has received increased attention in recent years, fuelled in part by the discovery² of high-temperature superconductivity in the doped cuprates. It is believed to play a key role in a number of recently observed phenomena, such as the large anomalous Hall effect in ferromagnetic pyrochlores³, the unconventional superconductivity in water substituted sodium cobaltate Na_xCoO_2 , which is composed of triangular sheets of Co atoms⁴, the interplay between magnetism and unconventional superconductivity in organic layered compounds of the κ -BEDT family^{5,6} or the interaction between electric and magnetic properties in multiferroic materials⁷.

The issue of frustration has been studied mostly on two classes of theoretical models: spin Hamiltonians, such as the J_1 - J_2 Heisenberg model discussed below, and toy dimer models, the latter inspired by P.W. Anderson's proposal⁸ of the resonating valence-bond (RVB) state as a possible explanation for high- T_c superconductivity.

One can view spin Hamiltonians as the large interaction, U , limit of the Hubbard model. It is thus of interest to study the effect of both interaction and frustration on the phase diagram. In this work, we study systematically the frustrated Hubbard model at half-filling on a square lattice with nearest t and next-nearest neighbour t' hoppings, described by the Hamiltonian:

$$H = t \sum_{\langle i,j \rangle} c_i^\dagger c_j + t' \sum_{\langle\langle i,j \rangle\rangle} c_i^\dagger c_j + U \sum_i n_{i\uparrow} n_{i\downarrow}, \quad (1)$$

where c_i^\dagger , c_i are the electron creation and annihilation operators and $n_{i\sigma}$ is the particle number operator on site i . The interaction is represented by U . Next-nearest

neighbor hopping t' introduces frustration since, from a weak coupling point of view, it produces deviations from perfect nesting, and, from a strong-coupling point of view, it leads to an effective antiferromagnetic superexchange interaction J_2 that opposes the tendency of next-nearest neighbors to order ferromagnetically when nearest-neighbor superexchange J_1 is antiferromagnetic.

Our study of the phase diagram as a function of U/t and t'/t can also be understood as a study of the generalized zero-temperature phase diagram for high-temperature superconductors illustrated in Fig. 1. The thin parallelepiped represents schematically the region of parameter space where families of high-temperature superconductors appear. We are studying the zero-doping plane $\delta = 0$, where one normally encounters the insulating antiferromagnetic parents of high-temperature superconductors. We will see that d-wave superconductivity can also occur in this plane, so high-pressure studies might conceivably lead to the observation of d-wave superconductivity even at half-filling, provided the on-site interaction U/t is not too large. The generalized phase diagram also leads to insights into the nature of d-wave superconductivity, as we will see.

We use a quantum cluster approach, the so-called variational cluster approximation (VCA, sometimes referred to as the 'variational cluster perturbation theory')⁹. This method has already been used successfully for the high-temperature superconductors^{10,11,12}. Other quantum cluster methods that are extensions of dynamical mean-field theory (DMFT)¹³, such as cellular dynamical mean-field theory¹⁴ and dynamical cluster approximation¹⁵, have yielded comparable results^{16,17} for the same problem. On the anisotropic triangular lattice at half-filling, both VCA¹⁸ and CDMFT¹⁹ give a phase

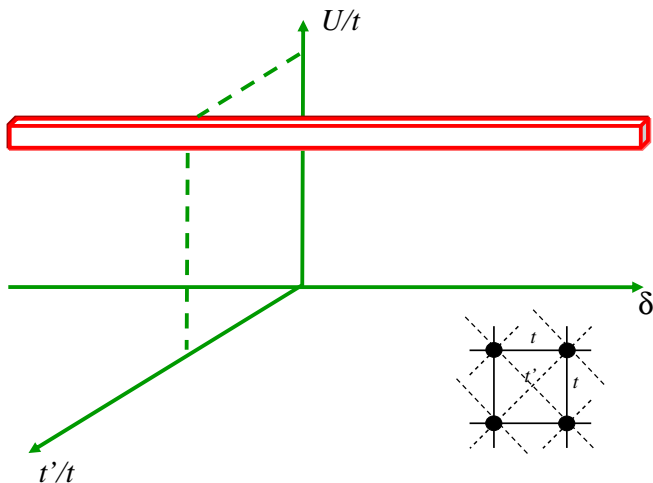


FIG. 1: (Color online) Schematic generalized zero-temperature parameter space for the high-temperature superconductors. Horizontal axis δ represents doping, vertical axis U/t interaction strength, and third direction t'/t frustration. The parallelepiped indicates the region of parameter space relevant for high-temperature superconductors. In this study, we consider the zero doping $\delta = 0$ plane. Experimentally, U/t can be varied by pressure. The inset shows the definitions of t and t' on the square lattice.

diagram that is in remarkable agreement with that of layered BEDT organic superconductors.

Wherever possible, we will make connections with earlier numerical studies on the half-filled square-lattice Hubbard model^{20,21}, and with work on spin-Hamiltonians.

This paper is organized as follows. First, the role of frustration in quantum magnets is illustrated in Section II on the well-studied example of the J_1 - J_2 Heisenberg spin model. The connection to the Hubbard model is then made by virtue of the large- U expansion in Section III. The framework of the variational cluster approximation (VCA) used in this work is briefly described in Section IV. The resulting magnetic phase diagram of the Hubbard model is then presented in Section V, with a separate subsection devoted to the analysis of the metal-insulator transition. The main result of this work, where d-wave superconductivity and magnetism compete and even coexist, is described in Section VI. We conclude by discussing the obtained phase diagram of the frustrated Hubbard model and draw comparison with other known results in Section VII.

II. A REFERENCE POINT: J_1 - J_2 HEISENBERG MODEL ON THE SQUARE LATTICE

One of the earliest studied models that exhibits frustration is the so-called J_1 - J_2 Heisenberg model, which contains antiferromagnetic (AF) spin-spin interaction between nearest and next-nearest neighbours (denoted by

$\langle i, j \rangle$ and $\langle\langle i, j \rangle\rangle$ respectively):

$$H = J_1 \sum_{\langle i, j \rangle} \mathbf{S}_i \cdot \mathbf{S}_j + J_2 \sum_{\langle\langle i, k \rangle\rangle} \mathbf{S}_i \cdot \mathbf{S}_k \quad (2)$$

Albeit simple in appearance, this model captures a number of important features common to a large class of frustrated quantum magnets.

Classically, the ground state of the model can be derived by considering the Fourier transform of the spin coupling $J(q)$, which on the square lattice with next-nearest neighbour spin interaction takes the following form:

$$J(q) = 2J_1(\cos q_x + \cos q_y) + 4J_2 \cos q_x \cos q_y. \quad (3)$$

The classical ground state should minimize this coupling, leading to two possible solutions: the Néel state (referred to as AF1 in the following) with the ordering wave-vector $\mathbf{Q} = (\pi, \pi)$ for the range of parameters $J_2/J_1 < 0.5$, and the so-called super-antiferromagnetic phase with $\mathbf{Q} = (\pi, 0)$ or $(0, \pi)$ (referred to as AF2), realised for $J_2/J_1 > 0.5$. Although non-collinear spin states with the same classical ground state energy can also be realized, it has been shown²² that thermal or quantum fluctuations will favour the states that have collinear magnetization.

The effect of quantum fluctuations becomes especially important around the quantum critical point $J_2/J_1 = 0.5$ where the classical ground state is highly degenerate. The large- S analysis shows²³ that even to the lowest order in $1/S$, zero-temperature quantum corrections to the sublattice magnetization diverge at the critical point, pointing to the existence of a quantum disordered phase. The nature of such a phase can be captured by dimer covering of the lattice, which is a caricature for the singlet pairings (i.e. valence bonds) of nearest-neighbour spins.

A wide literature²⁴ exists on the subject of spin rotationally invariant dimer order in frustrated quantum magnets. It is generally believed²⁴ that in the case of a square lattice, the dimer phase exhibits long-range order in the dimer-dimer correlation functions, leading to the notion of the ‘valence bond solid’ (VBS), as opposed to the original RVB phase of Anderson⁸ which is supposed to have only short-range order and gapped collective excitations. We shall touch upon this subject in Section V, although this study will be primarily concerned with the magnetic broken-symmetry phases.

III. LARGE- U EXPANSION OF THE $t - t' - U$ HUBBARD MODEL

In order to get insight into the physics of the frustrated Hubbard model, we shall first consider its large- U expansion. Whereas the procedure for obtaining the low-energy Heisenberg Hamiltonian from the conventional Hubbard model with nearest-neighbour interaction is a textbook example²⁵, the presence of next-nearest neighbour terms

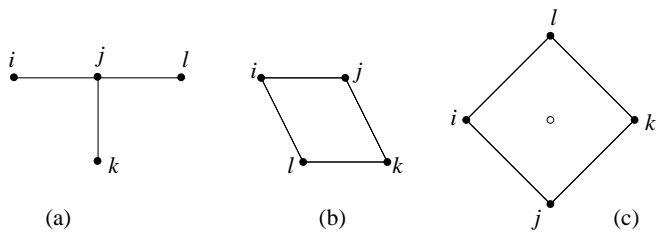


FIG. 2: The ring exchange contributions to the large- U expansion of the $t - t' - U$ Hubbard model from Ref. 26. The empty circle in case (c) denotes that the central site does not participate in the plaquette spin-exchange term.

and calculation to order $1/U^3$ leads non-trivial next-nearest-neighbor and ring-exchange terms. We exploit here the coefficients of the expansion that have been obtained by Delannoy *et al.*^{26,27} by means of the canonical transformation approach. The resulting effective spin Hamiltonian can be written as follows:

$$H = J_1 \sum_{\langle i,j \rangle} \mathbf{S}_i \cdot \mathbf{S}_j + J_2 \sum_{\langle\langle i,k \rangle\rangle} \mathbf{S}_i \cdot \mathbf{S}_k + \{\text{ring exchange terms}\} \quad (4)$$

where the coefficients J_i are given by

$$\begin{aligned} J_1 &= \frac{4t^2}{U} - \frac{24t^4}{U^3} + 4\frac{t^2t'^2}{U^3} + \dots; \\ J_2 &= \frac{4t^4}{U^3} + \frac{4t'^2}{U} - 8\frac{t^2t'^2}{U^3} + \dots \end{aligned} \quad (5)$$

The relevant ring exchange terms²⁶ are defined on the plaquettes depicted in Fig. 2 with the corresponding analytical expressions given by:

$$\begin{aligned} H_{(a)} &= 20J_{tt'}P_1(i, j, k, l) - J_{tt'}P_2(i, j, k, l) \\ H_{(b)} &= 20J_{tt'}P_1(i, j, k, l) + J_{tt'}P_2(i, j, k, l) \\ H_{(c)} &= 80\frac{t'^4}{U^3}P_1(i, j, k, l) - J_{tt'}P_2(i, j, k, l) \end{aligned} \quad (6)$$

where $J_{tt'} = 4t^2t'^2/U^3$ and the following notations have been used following Ref. 26:

$$P_1(i, j, k, l) = (\mathbf{S}_i \cdot \mathbf{S}_j)(\mathbf{S}_k \cdot \mathbf{S}_l) + (\mathbf{S}_i \cdot \mathbf{S}_l)(\mathbf{S}_k \cdot \mathbf{S}_j) - (\mathbf{S}_i \cdot \mathbf{S}_k)(\mathbf{S}_j \cdot \mathbf{S}_l) \quad (7)$$

$$P_2(i, j, k, l) = \{\mathbf{S}_i \cdot \mathbf{S}_j + \mathbf{S}_i \cdot \mathbf{S}_k + \mathbf{S}_i \cdot \mathbf{S}_l + \mathbf{S}_j \cdot \mathbf{S}_k + \mathbf{S}_j \cdot \mathbf{S}_l + \mathbf{S}_k \cdot \mathbf{S}_l\} \quad (8)$$

Evaluating the classical ground state energies of the Hamiltonian Eqs. (4-7) that corresponds to the two possible ordering wave-vectors $\mathbf{Q}_1 = (\pi, \pi)$ and $\mathbf{Q}_2 = (\pi, 0)$, yields the following result:

$$E_{(\pi,\pi)} - E_{(\pi,0)} = \frac{2t^2}{U} \left(-1 + \frac{8t^2}{U^2} - \frac{12t'^2}{U^2} + 2\frac{t'^2}{t^2} \right) \quad (9)$$

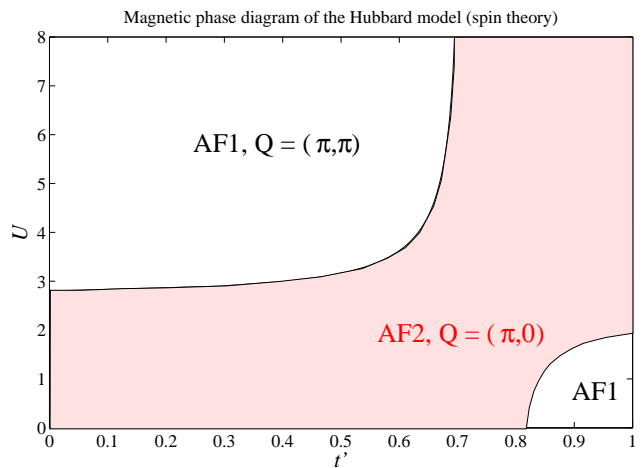


FIG. 3: (Color online) Classical phase diagram of the Hubbard model with next-nearest neighbour hopping t' based on the large- U expansion analysis. The usual AF phase (AF1) with the ordering vector (π, π) is observed at small ratios of t'/t , whereas a so-called super-antiferromagnetic phase $(0, \pi)$ (AF2, shaded region) is realized at large frustration t'/t . Note that because of the nature of the large- U expansion, this phase diagram is expected to be inaccurate at low U values.

The corresponding classical phase diagram that follows from this is shown in Fig. 3. Note that in the large of U limit, it follows from Eq. (9) that the criterion for the $(\pi, 0)$ phase to have lower ground state energy is given by $t'/t > 1/\sqrt{2}$, i.e. $J_2/J_1 > 0.5$, which coincides with the classical criterion obtained earlier for the J_1 - J_2 Heisenberg model.

Several comments on the phase diagram in Fig. 3 are due. First of all, the above analysis is based on the large- U expansion of the Hubbard model where electrons are localized. It should not be taken seriously for small U values where electrons can be delocalized even at half-filling. In particular, the AF2 $(\pi, 0)$ phase for a large range of t'/t below $U \lesssim 2.8t$ is an artifact. Secondly, the role of thermal and quantum fluctuations has been completely neglected in the above classical analysis. The latter are going to lower the ground state energies of the two AF phases but, more importantly, they may favour a different type of order with no broken rotational spin symmetry, such as the valence bond solid or the RVB spin liquid state mentioned earlier in relation with the J_1 - J_2 Heisenberg model.

Below, we take into account the effect of short-range quantum fluctuations at zero temperature as well as the possibility for electrons to delocalize. In order to achieve this we perform VCA calculations of the Hubbard model with nearest and next-nearest neighbour hopping and obtain the quantum analogue of the phase diagram shown in Fig. 3, including the possibility of d-wave superconductivity. These results are presented in Section V.

IV. VARIATIONAL CLUSTER APPROACH

Despite the apparent simplicity of the Hubbard model, its phase diagram is extremely rich in physical phenomena, such as antiferromagnetism, incommensurate spin-density wave and d-wave superconductivity. Analytical progress is severely hindered by the fact that the model does not have a small parameter in the interesting regime, and, consequently, a number of numerical methods have been proposed to treat the Hubbard model. Among these, quantum cluster methods²⁸ form a separate group, which seems to successfully capture many physical features of the model, including d-wave superconductivity that was studied^{10,16,17,29} in the context of the cuprates.

In this work we have used the so-called variational cluster approximation (VCA), sometimes referred to as variational cluster perturbation theory (VCPT) in the literature. It is a special case of the self-energy functional approximation^{30,31}. The idea of this approach consists in expressing the grand canonical potential Ω of the model as a functional of the self-energy Σ :

$$\Omega[\Sigma] = F[\Sigma] - \text{Tr} \ln (-G_0^{-1} + \Sigma), \quad (10)$$

where G_0 is the bare single-particle Green's function of the problem and $F[\Sigma]$ is the Legendre transform of the Luttinger-Ward functional, the latter being defined by the infinite sum of vacuum skeleton diagrams.

The functional (10) can be proven to be stationary at the solution of the problem, i.e. where Σ is the physical self-energy of the Hubbard model,

$$\left. \frac{\delta \Omega[\Sigma]}{\delta \Sigma} \right|_{\text{sol}} = 0. \quad (11)$$

The problem of finding the solution is then reduced to minimizing the functional $\Omega[\Sigma]$ with respect to the self-energy Σ . Two problems stand in the way however. Firstly, the functional $F[\Sigma]$ entering Eq. (10) is unknown and thus has to be approximated in some way. And secondly, there is no easy practical way of varying the grand potential with respect to the self-energy.

Potthoff suggested³⁰ an elegant way around these problems by noting that since the functional $F[\Sigma]$ is a universal functional of the interaction part of the Hamiltonian only (i.e. the last term in Eq. (1)), it can be obtained from the known (numerical) solution of a *simpler* reference system with the Hamiltonian H' defined on a partition of the infinite lattice into disjoint clusters, provided that the interaction term is kept the same as in the original Hamiltonian. For such a cluster partition, Eq. (10) can now be rewritten as

$$\Omega'[\Sigma] = F[\Sigma] - \text{Tr} \ln (-G_0'^{-1} + \Sigma), \quad (12)$$

where the prime denotes the quantities defined on the cluster, to distinguish from those of the original problem. Combining Eqs. (10) and (12), we finally obtain

$$\Omega[\Sigma] = \Omega'[\Sigma] + \text{Tr} \ln (-G_0'^{-1} + \Sigma) - \text{Tr} \ln (-G_0^{-1} + \Sigma). \quad (13)$$

Equation (13) is the central equation of the variational cluster approximation. The role of variational variables is played by some one-body parameters $\{h'\}$ of the cluster Hamiltonian, so that one looks for a stationary solution

$$\frac{\partial \Omega}{\partial h'} \equiv \frac{\delta \Omega[\Sigma]}{\delta \Sigma} \frac{\partial \Sigma}{\partial h'} = 0. \quad (14)$$

It has been shown by Potthoff³⁰ that the VCA and another widely known method, cluster dynamical mean field theory (CDMFT), can both be formulated in the framework of the above self-energy formalism. The particular advantage of the VCA is that it enables one to easily study broken-symmetry phases for clusters of varying sizes. The Weiss fields h' are introduced into the cluster Hamiltonian and the potential Ω is minimized with respect to it. It is important to stress that, in contrast with the usual mean-field theories, these Weiss fields are *not* mean fields, in a sense that the interaction part of the Hamiltonian is not factorized in any way and short-range correlations are treated exactly. The Weiss fields are introduced simply to allow for the possibility of a specific long-range order, without ever imposing this order on the original Hamiltonian.

In this work we have defined the cluster Hamiltonian with appropriate Weiss fields as follows:

$$H' = \sum_{\mathbf{x}, \mathbf{x}', \sigma} t_{\mathbf{x}\mathbf{x}'} c_{\mathbf{x}\sigma}^\dagger c_{\mathbf{x}'\sigma} - \sum_{\mathbf{x}, \mathbf{x}'} \left(\tilde{\Delta}_{\mathbf{x}\mathbf{x}'}^\dagger c_{\mathbf{x}\uparrow} c_{\mathbf{x}'\downarrow} + h.c. \right) - \tilde{M} \sum_{\mathbf{x}, \sigma} e^{i\mathbf{Q}\mathbf{x}} (-1)^\sigma n_{\mathbf{x}\sigma} - \mu' \sum_{\mathbf{x}\sigma} n_{\mathbf{x}\sigma} + U \sum_{\mathbf{x}} n_{\mathbf{x}\uparrow} n_{\mathbf{x}\downarrow} \quad (15)$$

Here as before, $c_{\mathbf{x}\sigma}^\dagger$ is the electron creation operator at site \mathbf{x} with spin σ , $n_{\mathbf{x}\sigma}$ is the particle number operator, and \tilde{M} and $\tilde{\Delta}_{\mathbf{x}\mathbf{x}'}$ are the Weiss fields corresponding to the antiferromagnetic order parameter (with ordering wave-vector Q) and to the superconducting order parameters respectively. For singlet superconductivity we have $\tilde{\Delta}_{\mathbf{x}\mathbf{x}'} = \tilde{\Delta}_{\mathbf{x}'\mathbf{x}}$. In particular, for $d_{x^2-y^2}$ symmetry the Weiss field is defined as follows (\mathbf{e} is a lattice vector):

$$\tilde{\Delta}_{\mathbf{x}, \mathbf{x}+\mathbf{e}} = \begin{cases} \tilde{D}, & \text{for } \mathbf{e} = \pm \hat{x} \\ -\tilde{D}, & \text{for } \mathbf{e} = \pm \hat{y}. \end{cases} \quad (16)$$

The corresponding order parameters, M and D , are given by the terms multiplying \tilde{M} and \tilde{D} respectively in the Hamiltonian (15).

In addition to the AF and SC Weiss fields, we also allow the cluster chemical potential μ' to vary, to insure internal thermodynamic consistency³² of the calculation. Therefore, in all calculations reported in the present work, the cluster chemical potential μ' was treated as a variational parameter, along with symmetry-breaking Weiss fields, such as the staggered magnetization in the AF case.

We solve the cluster problem using the Lanczos exact diagonalization technique, which enables one to find the ground state of the model at zero temperature. The cluster Green's function $G'_{ab}(\omega, \mathbf{k})$, defined for a pair of

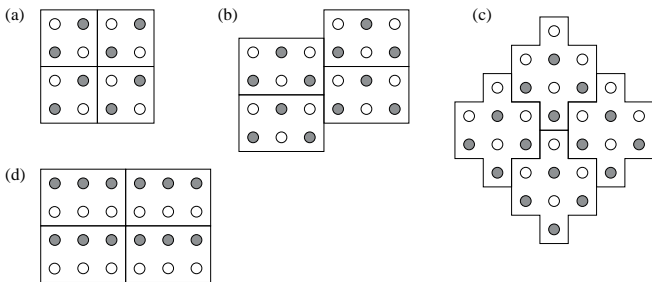


FIG. 4: The tilings of the square lattice with the various clusters used in this work containing (a) 4 sites, (b) 6 sites, (c) 8 sites. In this example the grey and white sites are inequivalent since the (π, π) AF order is possible. Note that in some cases, such as that of the 6-site cluster, a different tiling (d) must be chosen for a $(0, \pi)$ phase to become possible.

cluster sites (a, b), was then evaluated using the so-called band Lanczos method³³ that offers a significant computational advantage over other approaches³⁴. The search for a stationary solution Eq. (14) was performed using a combination of the Newton-Raphson³⁶ and the conjugate gradient methods³⁶.

Since all the calculations are performed in the grand-canonical ensemble, the requirement on the filling $\langle n \rangle = 1$ is achieved by choosing the appropriate value of the lattice chemical potential μ . We note that this task is not trivial in the present study since the variation of both the cluster chemical potential μ' and the Weiss field (the SC \tilde{D} and AF \tilde{M}) tend to greatly influence the value of $\langle n \rangle$. The appropriate value of the lattice chemical potential μ therefore had to be chosen at each point in the phase space of the parameters t, t', U of the Hamiltonian (1) to guarantee that the system always remained at half-filling.

In general the phase diagram will depend on the choice of the reference cluster system H' that is solved numerically to obtain the quantities entering the VCA equation (13). The VCA solution becomes exact only in the thermodynamic limit of infinitely large cluster. In practice, the typical cluster size is limited to a maximum of 10-12 sites since the Hilbert space of the reference cluster Hamiltonian grows exponentially with the cluster size and so does the computational cost of the exact diagonalization algorithm. In this work we have studied clusters of 4, 6 and 8 sites, as depicted in Fig. 4. This appears sufficient to suggest what the result should look like in the thermodynamic limit.

V. MAGNETISM AND MOTT PHYSICS IN THE FRUSTRATED HUBBARD MODEL

A. Magnetic phase diagram

When applying the VCA method to the frustrated Hubbard model, we have studied the possibilities for both

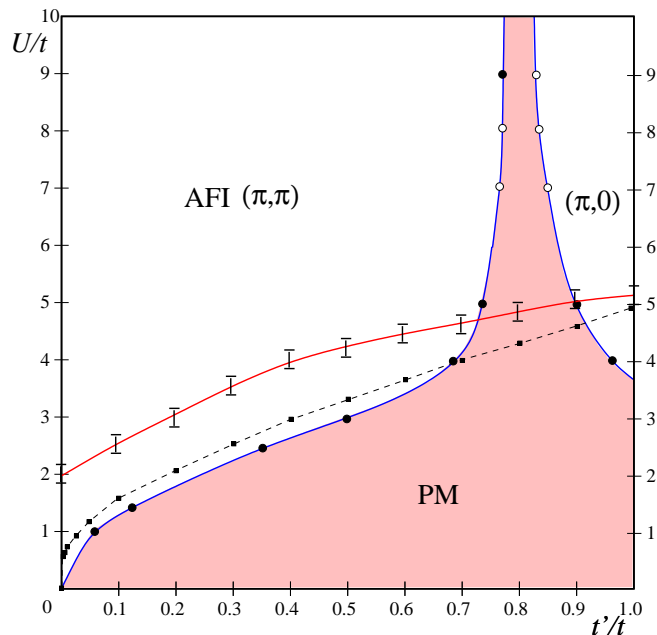


FIG. 5: (Color online) The magnetic phase diagram of the $t-t'-U$ Hubbard model ignoring the SC solution. There are two magnetic phases: (π, π) , $(\pi, 0)$ and the paramagnetic region (shaded area) where both order parameters vanish. The diagram was obtained with the VCA method using an 8-site cluster. The dashed line with filled data points shows the Hartree-Fock prediction from Ref. 37 for the transition between the Néel (π, π) and the non-magnetic phases. The solid line (red online) with error-bars indicates the transition $U_c(t')$ between the insulating (Mott-like) phase above and the metallic region below U_c when no magnetic order is allowed.

long-range magnetic order and (d-wave) superconductivity. In order to shed more light on the interplay between frustration and magnetism and to connect with existing studies on spin Hamiltonians summarized in Sec. II, we first report our results for purely magnetic phases, i.e. ignoring the SC solution for the moment. The main results of this study can be summarized by the phase diagram in Fig. 5 where the horizontal axis is a measure of the frustration t'/t and the vertical axis the interaction strength U/t .

We have looked for the same two AF phases that are predicted by both the J_1 - J_2 Heisenberg model (Sec. II) and the large- U expansion of the Hubbard model (see Sec. III), namely the usual Néel phase with the ordering wave-vector $Q = (\pi, \pi)$ and the so-called collinear order with $Q = (\pi, 0)$ (or equivalently, $(0, \pi)$). The regions of stability of these two phases are shown on the phase diagram in Fig. 5 for the largest cluster studied (8 sites). The two magnetic phases are separated by a paramagnetic region (filled area in Fig. 5) where no non-zero value was found for either of the two order parameters. We shall refer to this paramagnetic region as “disordered” although, strictly speaking, we cannot exclude the possibility of some other magnetic long-range

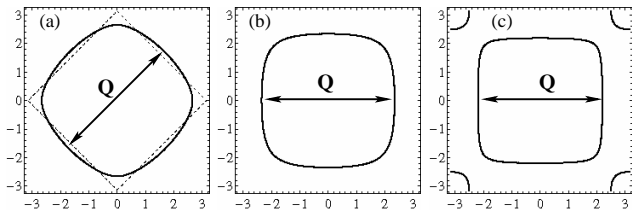


FIG. 6: Fermi surface for $t' = 0.2t$ (left), $t' = 0.6t$ (center) and $t' = 0.8t$ (right). The change in topology (Lifshitz transition) occurs around $t' = 0.71t$. The best nesting vector \mathbf{Q} is also shown. The Fermi surface for negative t'/t looks like the ones above if one translates the origin to (π, π) . The phase diagram in other figures depends only on the absolute value of t'/t .

order with, for example, incommensurate wavevector \mathbf{Q} , which is not tractable by our method because of the finite cluster sizes³⁵.

As is clear from Fig. 5, for large U values the disordered region is centred around the critical value $t'/t = 1/\sqrt{2}$, confirming the predictions of the large- U expansion (c.f. Fig. 3). This region then becomes broader as U is lowered, engulfing the whole of the phase diagram in the limit of $U = 0$. This is quite different from the semiclassical phase diagram of Fig. 3, that predicts that the AF2 phase should be more stable below $U \lesssim 2.8t$ for a broad range of t' values. This discrepancy is however not surprising given that the classical phase diagram was obtained from the large- U expansion that is bound to fail in the small- U region of the phase diagram.

One should note that around $t'/t = 1/\sqrt{2}$ the topology of the non-interacting Fermi surface changes, as depicted in Fig. 6. This figure suggests why the ordering wave vectors take the above mentioned values.

It is instructive to compare the transition into the Néel phase obtained here, with the known Hartree-Fock result for the half-filled Hubbard model³⁷ (dashed line in Fig. 5). The VCA results follow closely the Hartree-Fock results for $t' < 0.7$, whereas for higher levels of frustration, the non-trivial disordered region is revealed by VCA, followed by the $(\pi, 0)$ magnetic phase (the latter was not considered by the authors of Ref. 37).

We note that all the transitions on the phase diagram have been found to be first order (with a possible exception of very low U values where a reliable solution is progressively harder to obtain). By this we mean that the magnetic order parameter jumps as the transition line is crossed, so that either no magnetic solution was found in the PM phase (typical the low U region) or alternatively, since hysteresis is expected, its free energy was found to be actually higher than that of the PM solution (typically the case for $U/t > 6$).

The two AF phases mentioned above, (π, π) and $(\pi, 0)$ have been found not only in studies of the J_1 - J_2 Heisenberg model, as already mentioned, but also in work on the frustrated Hubbard model by Mizusaki and Imada²¹.

There, the $(\pi, 0)$ phase is, perhaps confusingly, called a “stripe” phase. By using a path-integral Monte-Carlo technique, they found a phase diagram very similar to ours. In addition, these authors find a third phase with a larger periodicity in real space corresponding to the ordering vector $\mathbf{Q} = (\pi, \pi/2)$, which exists in a narrow region of t'/t between 0.6 and 0.8 for $U \gtrsim 7$. This is precisely the region where neither $(\pi, 0)$ nor (π, π) phases have been found stable in this work. It may well be that another magnetically ordered phase (probably incommensurate³⁵) exists in this intermediate region. Unfortunately, the clusters used in this work, see Fig. 4, are not suitable to check for the stability of the $(\pi, \pi/2)$ phase.

Apart from the possibility of some non-trivial magnetic order, the question remains open whether the ‘disordered’ phase around $t'/t = \sqrt{2}$ can actually be formed by spin singlets sitting on bonds, as e.g. in the so-called valence-bond solid (VBS). This phase is characterised by spontaneously broken translational symmetry, but preserves the spin-rotational symmetry and is considered to be the most likely candidate for the intermediate phase around the boundary between the two magnetic phases of the J_1 - J_2 Heisenberg model (see Ref.24 and references therein). Another possibility is the spin liquid phase, which is similar to VBS, but preserves the translational invariance of the system and can be interpreted as a resonating valence bond (RVB) state.

As it stands, the VCA approach does not permit to study the various possibilities for a VBS or spin liquid phase. Therefore, at present, we cannot judge whether such an order may exist in the paramagnetic region or how far it extends into the low- U part of the phase diagram. It is interesting that a quantum spin liquid state has been recently shown to exist in the Hubbard model on a square lattice at half filling by numerical studies on finite clusters²¹ using path-integral Monte-Carlo method³⁸. This state, observed in a narrow region of U/t values between 4 and 7, falls between the metallic paramagnetic state and the magnetic insulator and is believed to be caused by charge fluctuations in the vicinity of the Mott transition (see more on that in Sect. VB). Unlike in the magnetically ordered state, the quantum spin liquid is characterized by the absence of any sharp peaks in the spin correlation function $S(\mathbf{q})$. It is certainly an intriguing possibility that should be verified with other existing numerical methods.

Naturally, if the VBS or quantum spin liquid solution happens to have a lower energy than either of the two magnetic phases discussed in this work, this would lead to further enlargement of the range of t' values where no long-range magnetic order is found. In this sense the VCA method only gives a lower bound on the extent of the non-magnetic hatched region in Fig. 5, which for e.g. $U/t = 9$ exists in the range of $0.77 < t'/t < 0.82$. It is useful to compare these figures with the exact diagonalization results³⁹ for the J_1 - J_2 Heisenberg model discussed in Sec. II: There, the non-magnetic region ap-

pears in the range $0.4 \lesssim J_2/J_1 \lesssim 0.6$. For the Hubbard model, this translates into the large U limit and the window $0.63 \lesssim t'/t \lesssim 0.78$, which is indeed much wider than predicted by VCA.

B. Metal-insulator transition

We next turn to the subject of the metal-insulator transition in the frustrated Hubbard model at half-filling in the absence of long-range order. Since there is no bath in VCA as we define it, metallic states are less favored than in CDMFT. In the normal state, the bath present in CDMFT or DMFT can play the role of a metallic order parameter. While metallic states can occur in VCA, they cannot occur as first order transitions because of the absence of this metallic order parameter. So, contrary to the case of CDMFT^{19,40}, the Mott transition cannot be observed as a cusp or discontinuity in the site double occupancy $\langle n_{\uparrow}n_{\downarrow} \rangle$ – the dependence of this quantity on U/t is a very smooth monotonic curve.

The Mott transition is however firmly established in the half-filled Hubbard model, and can indeed be observed by analyzing the spectral function $A(\mathbf{k}, \omega)$. Therefore, for the purpose of this study, we define a “metal” as a state with non-vanishing spectral function at the Fermi level, $A(\mathbf{k}, \omega = 0)$. We note in passing that the latter definition is actually broader than saying that there exists a well-defined Fermi surface in the ground state, for the following reasons. Firstly, the regions of non-vanishing $A(\mathbf{k}, \omega = 0)$ need not form a closed surface, but may instead have a shape of isolated arcs (c.f. the well-known Fermi arcs as revealed by ARPES spectroscopy⁴¹ in the underdoped cuprates). Secondly, the Landau picture of a metal predicts an infinite lifetime for the quasiparticles at the Fermi surface, equivalent to the requirement of delta-function shape for $A(\mathbf{k}, \omega = 0)$ at the Fermi energy.

Since the presence of a long-range magnetic order opens up a gap at the Fermi surface, we intentionally suppress the possibility of magnetic ordering. Only the effect of short-range magnetic correlations is included in the cluster. This is an established practice used to obtain the parameters of the metal-insulator transition^{19,28,29,40}.

The procedure we have adopted is as follows. For a given value of t' , we plotted the function $A(\mathbf{k}, \omega = 0)$ across the Brillouin zone (BZ) for several values of the interaction U , with the Lorentzian broadening $\eta = 0.05$ used to account for the imaginary part of $A(\mathbf{k}, \omega)$. The point where the spectral function vanishes everywhere in the BZ (as U is increased) marks the transition from metallic to insulating state. In the present approach, the transition appears as a crossover, that strictly speaking at zero temperature should be a second-order transition. On the anisotropic triangular lattice, it was found that as a function of t' , the Mott transition goes from second order at small t' to strongly first order at large t' through a tricritical point^{19,42}.

Our “crossover” transition line together with error bars is plotted in Fig. 5. We see that with increasing frustration t' , the critical value $U_c(t'/t)$ increases monotonically. We note an important difference between the low- t' region and that for $t' \gtrsim 0.7t$. In the former case of almost perfect nesting, the effect of short-range correlations is strong, leading to a surprisingly low value of $U_c \approx 2t$. At first sight, this is too different from the well-known DMFT result¹³ for the Mott metal-insulator transition, $U \approx 12t$. It must be noted however that the single-site DMFT approach¹³ does not take into account short-range magnetic correlations, as opposed to cluster methods such as CDMFT or VCA. In addition, to study the Mott transition, DMFT assumes the presence of large frustration to prevent magnetic long-range order. Hence, the DMFT result should be compared with the region $t' \gtrsim 0.7t$ in our phase diagram Fig. 5 where magnetic order is naturally absent and the critical interaction strength is $U_c \approx 5t$. In real experiments, that is where we believe true Mott physics would be observed. In any case, it is physically expected that in two dimensions the critical U for the Mott transition depends on frustration, as pointed out in CDMFT study of the anisotropic triangular lattice¹⁹.

It is encouraging that values of $U_c(t'/t)$ very similar to ours have been found in the path-integral Monte-Carlo study²¹ of the same model, yielding $U_c = 3t$ at $t'/t = 0.25$ and $U_c = 5t$ for $t'/t = 0.8$. However, the authors of Ref. 21 have not excluded the possibility of long-range magnetic order, which is why they observe the Mott transition happening at infinitesimally small values of U in the case of perfect nesting $t' = 0$. We stress that this is in complete agreement with our data, although we interpret this as an opening of the AF gap at the Fermi surface rather than Mott transition into a phase with no broken spin-rotational symmetry. A somewhat poorer agreement is seen with the results of the optimized variational Monte Carlo (VMC) method in Ref. 20. There, the authors obtain the value $U_c \approx 7t$ in the region $|t'/t| < 0.5$ that they studied.

Our value of $U_c \lesssim 5t$ around $t'/t = 0.7$ should also be compared with the recent CDMFT results for strongly frustrated lattices, such as the triangular lattice⁴³ with $U_c = 10.5t$ and the asymmetric square lattice¹⁹ ($t' = t$ along only one diagonal) with $U_c \approx 8t$. Although CDMFT predicts higher U values for the Mott metal-insulator transition than VCA in these cases, they clearly fall into the same ballpark. However, for the square lattice without frustrations ($t' = 0$) the 4-site cluster CDMFT gives a value⁴² for the Mott transition $U_c \approx 5t$, quite a bit larger than our result $U_c \approx 2t$. Similar to CDMFT, a value $U_c \approx 6t$ was also found in Quantum Monte Carlo studies⁴⁴ at $t' = 0$. This discrepancy is however not surprising since it is well known⁴², for the reasons mentioned at the beginning of this section, that VCA method (without a bath) tends to overestimate the effect of interactions compared with CDMFT, thereby yielding smaller values of U_c for the Mott transition.

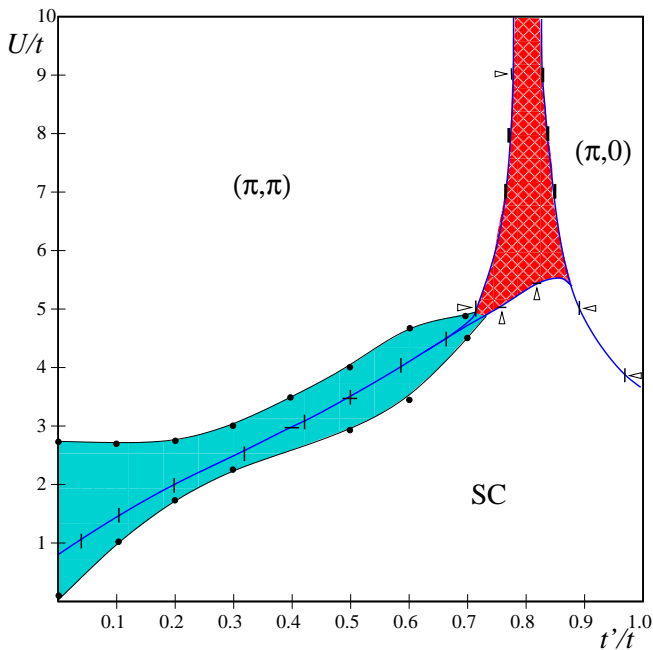


FIG. 7: (Color online) The phase diagram of the $t - t' - U$ Hubbard model obtained with the VCA based on a 8-site cluster. The solid lines denote the phase boundaries between the (π, π) and $(\pi, 0)$ antiferromagnetic phases and the $d_{x^2-y^2}$ SC phase. The hatched area on the phase diagram (red-and-white online) denotes the critical region where neither (π, π) nor $(\pi, 0)$ order could be found. The coexistence region between AF and SC phases (shaded area, cyan online) is contained between two black lines that meet around $t' = 0.7t$, with the (blue) line in between indicating the area where the free energies of the would-be separate SC and AF phases become equal (c.f. the point $U = 2.45t$ in Fig. 8b). Triangles and filled circles denote points on the phase boundary where an order parameter sustains a discontinuity at a first-order phase transition; short dashes inside the coexistence region mark the points where total energies of the AF and SC phases are equal.

VI. INTERPLAY BETWEEN MAGNETISM AND SUPERCONDUCTIVITY

A. Results and discussion

Our final VCA phase diagram is shown in Fig. 7 for the largest 8-site cluster studied. Most interestingly, in addition to the two magnetic phases discussed in the previous section, a d-wave superconducting solution (with $d_{x^2-y^2}$ symmetry) comes out naturally from the VCA calculations for low values of U/t in the phase diagram. It is clear from Fig. 7 that the frustration tends to destroy the Néel phase and stabilise the SC solution. In the whole range $|t'/t| < 1$, we did not find any superconducting regions with stable d_{xy} symmetry of the order parameter, although there are indications³⁵ that such a phase would become stable in the case of (unrealistically large)

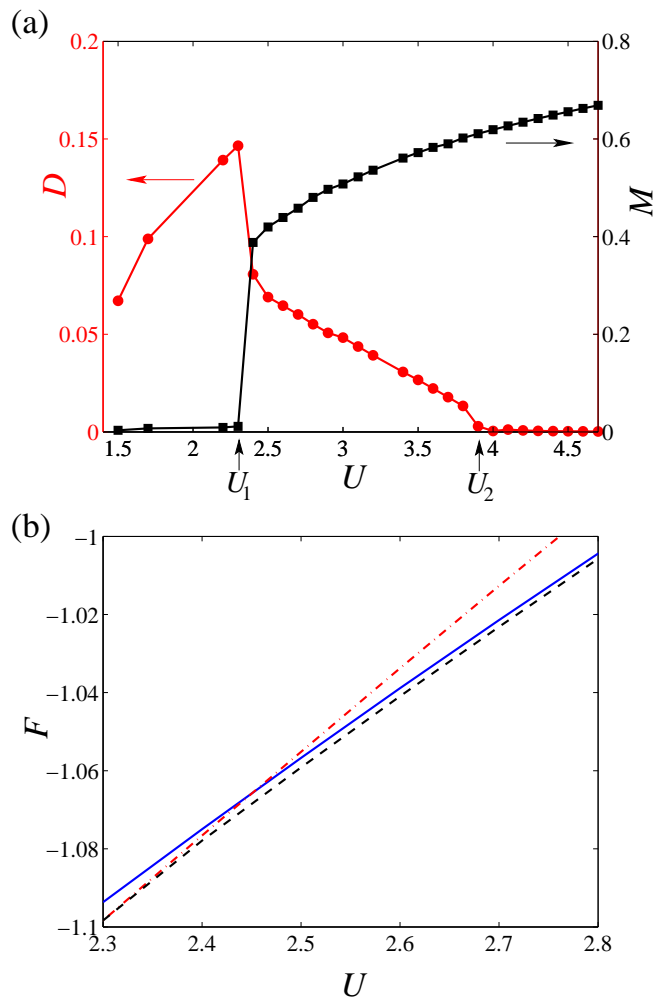


FIG. 8: (Color online) Details of the AF and SC phase coexistence for a 2×3 cluster at $t' = 0.2t$. (a) Expectation values of SC (D , circles and red line) and AF (M , squares and black line) order parameters as a function of increasing interaction U ; note different scales for the two quantities plotted. Values U_1 and U_2 denote the positions of the first-order phase transitions into/from the coexistence phase. (b) Blow up of the free energy $F = \Omega + \mu\langle n \rangle$ as a function of U near $U = 2.5t$ is shown for all three phases studied: AF phase (blue solid line), SC phase (red dash-dotted line) and for the coexistence phase where both D and M order parameters are non-zero (dashed black line). The latter phase has lower energy than the other two in the whole coexistence region of $2.3 < U/t < 3.9$.

frustration strength $t'/t \gtrsim 1.1$.

In the low- U region of the phase diagram, both AF and d-wave SC solutions are stable, hence the one with lowest free energy F would win. Since we work at a fixed particle density n (half-filling), we perform the Legendre transform to obtain the free energy from the grand-canonical potential Ω :

$$F \equiv E - TS = \Omega + \mu\langle n \rangle. \quad (17)$$

Moreover, since the calculations are done at zero temper-

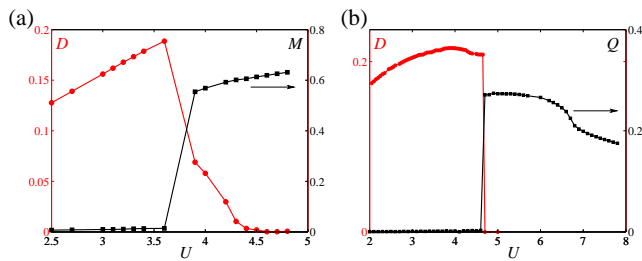


FIG. 9: (Color online) The expectation values of SC (D , circles and red line, left-hand scale) and two types of AF order parameters (shown with squares and black lines), calculated on a 2×3 cluster for (a) $t' = 0.5t$, the AF (π, π) phase order parameter M (right-hand scale), and (b) $t' = 0.8t$, the $(\pi, 0)$ phase order parameter Q (right-hand scale). Unlike in (a), no coexistence region is seen in case (b), where the first-order transition occurs at $U_c = 4.7t$.

ature, the Gibbs free energy in this case is identical to the total energy E of the system. We find that the transition between the magnetic and the SC phases is first order, with the blue line in Fig. 7 (in the centre of the shaded region) denoting the points where the total energies of the two competing phases (no coexistence allowed) become equal. The free energy of both phases is illustrated in more detail by the dot-dashed and solid lines in Fig. 8b.

Most interestingly, the lowest energy solution (dashed line in Fig. 8b) corresponds to a new phase, shown as shaded area in Fig. 7, where both magnetic and SC order parameters are non-zero. This is a phase with a true *homogeneous coexistence* of the magnetic and superconducting phases, which one may want to call an *antiferromagnetic superconductor* to emphasize the difference from a more usual inhomogeneous coexistence observed e.g., at a first-order transition.

The details of the transition between the coexistence phase and the pure AF and SC phases are illustrated in Figs. 8a and Fig. 9a that show the dependence of the corresponding order parameters, M and D , on the interaction strength U . As U decreases below U_1 in Fig. 8a, we first observe a first-order transition from the coexistence phase into a pure d-wave SC state, where the AF order parameter plunges to zero and the SC order parameter sustains an upward jump as the coexistence phase ceases to exist. As the interaction increases above $U = U_2$, there is a similar transition from the coexistence phase into the pure antiferromagnet (π, π) , although this time the transition appears more continuous (see Fig. 8a).

Clearly, our phase diagram Fig. 7 shows that frustration t'/t favors the SC phase as long as it is not too large. Indeed SC becomes more stable and occupies a broader region of the phase diagram as frustration increases at low to intermediate interaction strength U , until t'/t becomes large enough for the AF2 $(\pi, 0)$ phase to decrease the area occupied by the SC phase. The latter transition is of first order and is accompanied by a sharp jump in the values of the respective order parameters at $U = U_c$,

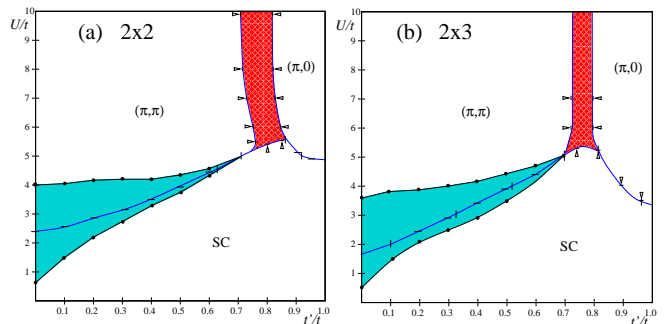


FIG. 10: (Color online) The phase diagram of the $t - t' - U$ Hubbard model obtained with the VCA based on an (a) 4-site cluster and (b) 6-site cluster. The hatched area (red-and-white online) denotes the critical region where neither (π, π) nor $(\pi, 0)$ order could be found or when the paramagnetic solution had lower energy than any of the AF phases. The coexistence region between SC and AF phases (shaded area, cyan online) is shown. The solid lines, as well as open triangles and short dashes on the phase boundaries have the same meaning as in Fig. 7.

as one can verify on Fig. 9b for $t'/t = 0.8$ for the 6 site cluster. Sometimes a very narrow hysteresis region ($\Delta U/t \lesssim 0.2$) has been observed, depending on whether the transition is approached from above or below the critical value of U_c .

In the region of $t'/t \approx 0.75$ of the phase diagram Fig. 7, the SC phase has a direct boundary with the disordered non-magnetic phase as a function of increasing U . Given the possibility for the existence of the VBS order in that region, this opens up the interesting possibility of a direct transition from VBS into the SC state. Since the two phases have symmetry groups that are not related to each other, according to Landau theory they would be separated either by a first order transition or by a coexistence phase. Or, beyond the Landau paradigm, they could lead to an example of deconfined quantum criticality⁴⁵. A similar deconfined critical transition could also possibly occur between the VBS and antiferromagnetic phases.

To assess convergence towards the thermodynamic limit, it is useful to compare the phase diagrams obtained for different cluster sizes. Figure 10 shows the VCA phase diagrams obtained from the 4-site and 6-site clusters. We see that the main conclusions, namely that the d-wave SC phase is the ground state for low U values, remains unchanged. However the position of the AF1-SC phase boundary shifts to lower U values with increasing cluster size. This is to be expected since perfect nesting at $t' = 0$ and half-filling should lead to antiferromagnetism as the true ground state of the Hubbard model at arbitrary small values of U . This suggests that perhaps the coexistence of SC and AF1 at small $t' = 0$ should disappear altogether in the thermodynamic limit of infinitely large cluster size. We do see from Figs 10 and 7 a decrease in the size of the coexistence region as the

cluster size increases.

We also note that the phase boundary of the collinear $(\pi, 0)$ phase occurs at lower values of U with increasing cluster sizes. For example, comparing Figs. 10 and 7, we see that at $t'/t = 0.96$ the transition from the AF2 phase into the SC phase occurs at $U/t \approx 3.5$ for the 8-site cluster instead of $U/t \approx 5$ that one observes for the smallest cluster studied. As in the case of the largest cluster studied (phase diagram in Fig. 7 above), all transitions between the different phases, including the coexistence phase between AF and SC orders, were found to be first order.

We now compare our phase diagram in Fig. 7 with that found by other methods. Recently, the path-integral Monte Carlo study of the same model by Mizusaki and Imada²¹ has revealed a phase diagram where the magnetic and PM regions are in very good agreement with our Fig. 5, apart from an extra magnetic phase that the authors of Ref. 21 observe between the AF and the $(\pi, 0)$ phases. This however does not contradict our results since even more complicated phases, such as incommensurate magnetic order, may be possible but are beyond reach of quantum cluster methods such as VCA. Another important difference is the existence of the quantum spin liquid phase found in Ref. 21 that we commented upon in Sect. V A. The possibility of superconducting phase has not been addressed however in Ref. 21. This would have been very instructive in light of our findings.

Another recent study of the half-filled Hubbard model has been performed recently by Yokoyama *et al.*²⁰ using optimization VMC. They considered both the (π, π) AF phase and $d_{x^2-y^2}$ superconductivity. It is puzzling that the AF phase has been found to be limited to the region $|t'/t| < 0.2$ only, in contradiction with both our work and the known results of the J_1 - J_2 model in the strong coupling limit. As the authors themselves suggest, this discrepancy is most likely due to a bad choice of the variational state and/or the limitations of the VMC method. In that work, the d-wave SC state is found to be most stable in the vicinity of the Mott transition ($U_c = 6.7t$) for a narrow range of $0.2 < |t'/t| < 0.4$, although the authors mention that a small magnitude of the SC gap survives often to very small values of U/t , which would be in agreement with our results showing that SC exists in the whole region of $0 < |t'/t| < 1$ down to $U = 0$. Unfortunately, the limited range of $|t'/t| < 0.5$ studied in Ref. 20 does not help to shed light on the existence of other AF orderings, such as the $(\pi, 0)$ state, or indeed on the long sought after quantum spin liquid state, claimed to have been observed convincingly in Ref. 21.

B. Comparison with results on the anisotropic triangular lattice

To conclude this section, we contrast the results with those obtained on the anisotropic triangular lattice^{18,19}. First of all, on that lattice CDMFT shows that phase

transitions between ordered phases occur at the same location as the Mott transition when the latter is first order¹⁹. This does not happen when the transition is second order⁴². In our case, the Mott transition is always second order and the transitions between ordered phases do not coincide with the Mott line as we can see by comparing the line with error bars on Fig. 5 with the phase diagram in Fig. 7.

On the anisotropic triangular lattice, the transition between d-wave superconductivity and antiferromagnetism is always first order with no coexistence region, in contrast with our case where (π, π) antiferromagnetism is separated from d-wave superconductivity by a coexistence phase. At larger frustration however, d-wave superconductivity is separated from $(\pi, 0)$ antiferromagnetism by a first order transition. Since the triangular lattice has geometric frustration, not only frustration induced by interactions, one can speculate that it is the larger frustration on the anisotropic triangular that leads to the disappearance of the coexistence phase. However, at $t' = 0$ both problems become identical and there is a clear disagreement between the results that can come only from differences in the two calculational approaches, CDMFT vs VCA.

It is rather striking that on the anisotropic triangular lattice, the d-wave order parameter is largest as a function of U/t when it touches the first order boundary with the antiferromagnetic phase. As can be seen from Figs. 8a and 9a, this also occurs in our case when d-wave superconductivity touches the homogeneous-coexistence phase boundary. Also, the maximum value of the order parameter increases in going from $t' = 0.2t$ to $t' = 0.5t$, as in the case of the anisotropic triangular lattice. At larger frustration, the trend as a function of t'/t reverses on the latter lattice. In our case, we see that at large frustration $t' = 0.8t$ on Fig. 9b, the d-wave order parameter reaches its maximum value before it hits the first order boundary with the $(\pi, 0)$ phase.

It would clearly be interesting to compare what are the predictions for our case of other quantum cluster approaches, such as CDMFT and DCA. The weak to intermediate coupling Two-Particle Self-Consistent Approach³⁵ suggests that at small values of U superconductivity disappears in favor of a metallic phase and that at $t' = 0$ antiferromagnetism dominates. We expect the predictions of VCA to be more reliable at strong coupling.

VII. SUMMARY AND CONCLUSIONS

We have analyzed the phase diagram of the half-filled Hubbard model as a function of frustration t'/t and interaction U/t using both analytical and numerical techniques.

The classical analysis based on the resulting large- U effective spin Hamiltonian allowed us to draw the classical magnetic phase diagram shown in Fig. 3. Of course, this

classical approach remains completely oblivious to the role of quantum fluctuations and in addition is designed for the high- U segment of the phase diagram where electrons are localized.

To treat quantum fluctuations as well as the possibility of delocalization, we used the Variational Cluster Approximation. Because of the nature of the VCA method, it relies on the choice of a finite (necessarily small) cluster on which the problem can be solved exactly. In order to the finite-size effects, we have analyzed the results for clusters of 4, 6 and 8 sites (the latter being almost at the limit of what can be achieved with today's powerful supercomputers using the exact diagonalization algorithm). Although the exponentially increasing computational cost did not permit us to study larger clusters, the apparent similarities between the 6- and 8-site cluster solutions allow us to conclude that the VCA calculations reported in this study are close to convergence with respect to increasing cluster size.

Independent of the cluster size used, the key features of the resulting phase diagram are as follows. At large values of U the VCA results agree qualitatively with the classical large- U expansion (Sec. III) of the Hubbard Hamiltonian and with the known results for the related J_1 - J_2 Heisenberg spin model (Sec. II), which show that two competing AF phases AF1 and AF2 with ordering wave-vectors $\mathbf{Q}_1 = (\pi, \pi)$ and $\mathbf{Q}_2 = (\pi, 0)$ exist for frustrations lower and higher, respectively, than some critical value given roughly by $t'_c/t = 1/\sqrt{2} \approx 0.71$. This is where the Fermi surface changes topology in the non-interacting case (see Fig. 6). These two magnetic phases are separated by a disordered region where we don't find non-zero values of either order parameter. The Heisenberg model studies point to possible existence of an exotic valence bond solid (VBS) phase around the critical frustration value t'_c . Although the direct study of the VBS phase remains beyond reach of quantum cluster methods such as VCA, it is encouraging that the obtained phase diagram exhibits a region around the critical frustration t_c where no long-range AF order could be found.

We have also addressed the issue of the role of frustration on the metal-insulator transition that is known to exist in the Hubbard model at half-filling. The distinction between metallic and insulating phases was based on the analysis of the spectral function $A(\mathbf{k}, \omega)$ at the Fermi level, which is vanishing in the insulating ground state. We find that the value of the interaction strength U_c where the insulator appears rises monotonically as a function of frustration strength t' . The value of U_c turns out to be surprisingly low for small t' values ($U_c \approx 2t$). Low values are expected from the effect of short-range antiferromagnetic fluctuations that are particularly strong near perfect nesting at $t' = 0$. Nevertheless, comparisons with other results definitely suggest that VCA overemphasizes the effect of U so that the insulator-metal transition at half-filling should be closer to the CDMFT and QMC values $U_c \approx 5 - 6t$. For large frustration near $t'_c/t = 1/\sqrt{2} \approx 0.71$, the transition occurs at larger val-

ues of $U_c \approx 5t$. Since neither the AF1 or AF2 phases are stable in this highly frustrated region, this is where one would experimentally be more likely to see a genuine Mott transition at finite temperature where ordered phases are absent.

Most importantly, the VCA method allowed us to study the region of the phase diagram with low to intermediate interaction strength, which is inaccessible in the large- U expansion or the J_1 - J_2 Heisenberg spin model. We find that even at half-filling, where the tendency towards the antiferromagnetic ordering is strong, frustration allows d-wave superconductivity to appear for a range of values of U/t that generally increases with frustration since the latter is detrimental to (π, π) antiferromagnetism. With frustration in the range $t'_c/t \approx 1/\sqrt{2}$, both (π, π) and $(\pi, 0)$ antiferromagnetism disappear but d-wave superconductivity survives for $U_c \lesssim 5t$. Increasing frustration further favors the $(\pi, 0)$ phase but d-wave superconductivity continues to appear at smaller values of U/t . All the phase transitions are first order, except possibly the transition from the coexistence phase into the (π, π) magnet, which is weakly first order (note a very small jump in the value of SC order parameter at the $U = U_2$ phase boundary in Fig. 8 a). In the case of (π, π) antiferromagnetism, the transition to pure d-wave superconductivity occurs through a region where both phases coexist homogeneously. Finite size analysis suggests that this coexistence region is relatively robust, although its boundaries shrink with increasing cluster size. Coexistence may disappear in the thermodynamic limit.

An important prediction of our study for experiments is that d-wave superconductivity may appear by applying sufficiently high pressure on the half-filled parent compounds of high-temperature superconductors. This type of transition is observed in layered BEDT organics⁵ and can be explained by the Hubbard model^{18,19}. Hence positive results of such an experiment on the cuprates would spectacularly help to establish definitively the electronic origin of d-wave superconductivity.

It would be interesting to pursue the issues addressed in this work with other quantum cluster approaches and also to study the case of doped Hubbard model away from half-filling, with possible comparison with the results of the much studied t - J model. Anticipating on the results, it should be easier to reach the d-wave superconducting state by applying pressure on a slightly doped insulating parent than on the half-filled insulator. These issues, of much relevance to the physics of high-temperature superconductivity in the cuprates, are left for future studies.

Acknowledgements

The authors are grateful to Raghieb Syed Hassan, Bumsoo Kyung, and Bahman Davoudi for many stimulating discussions. A.H.N. was supported by FQRNT. C.S. acknowledges partial support by the FWF (Project no. P18551-N16) and by KUWI grant of Graz Univer-

sity of Technology. Numerical computations were performed on the Dell clusters of the Réseau québécois de calcul de haute performance (RQCHP) and on Sherbrooke's Elix cluster. The present work was supported

by NSERC (Canada), FQRNT (Québec), CFI (Canada), CIFAR, and the Tier I Canada Research chair Program (A.-M.S.T.).

-
- * E-mail: nevidomskyy@cantab.net; Present address: Department of Physics and Astronomy, Rutgers University, 136 Frelinghuysen Road, Piscataway, NJ 08854, USA
- ¹ For an introduction to frustrated magnets see R. Moessner, *Can. J. Phys.* **79**, 1283 (2001).
 - ² J. G. Bednorz and K. A. Müller, *Z. Phys. B-Condens. Mat.* **64**, 189 (1986).
 - ³ Y. Taguchi, Y. Oohara, H. Yoshizawa, N. Nagaosa, and Y. Tokura, *Science* **291**, 2573 (2001).
 - ⁴ K. Takada *et al.*, *Nature* **422**, 53 (2003).
 - ⁵ S. Lefebvre *et al.*, *Phys. Rev. Lett.* **85**, 5420 (2000).
 - ⁶ Y. Kurosaki, Y. Shimizu, K. Miyagawa, K. Kanoda, and G. Saito, *Phys. Rev. Lett.* **95**, 177001 (2005).
 - ⁷ G. R. Blake *et al.*, *Phys. Rev. B* **71**, 214402 (2005).
 - ⁸ P. W. Anderson, *Science* **235**, 1196 (1987).
 - ⁹ M. Potthoff, M. Aichhorn, and C. Dahnen, *Phys. Rev. Lett.* **91**, 206402 (2003).
 - ¹⁰ D. Sénéchal, P.-L. Lavertu, M.-A. Marois, and A.-M. S. Tremblay, *Phys. Rev. Lett.* **94**, 156404 (2005).
 - ¹¹ M. Aichhorn and E. Arrighoni, *Europhys. Lett.* **72**, 117 (2005).
 - ¹² M. Aichhorn, E. Arrighoni, M. Potthoff, and W. Hanke, arXiv:0707.3557v1
 - ¹³ A. Georges, G. Kotliar, W. Krauth, and M. J. Rozenberg, *Rev. Mod. Phys.* **68**, 13 (1996).
 - ¹⁴ G. Kotliar, S. Y. Savrasov, G. Palsson, and G. Biroli, *Phys. Rev. Lett.* **87**, 186401 (2001).
 - ¹⁵ M. H. Hettler, A. N. Tahvildar-Zadeh, and M. Jarrell, T. Pruschke, H. R. Krishnamurthy, *Phys. Rev. B* **58**, R7475 (1998).
 - ¹⁶ S. S. Kancharla, M. Civelli, M. Capone, B. Kyung, D. Senechal, G. Kotliar, A.-M.S. Tremblay, cond-mat/0508205.
 - ¹⁷ T.A. Maier, M. Jarrell, T.C. Schulthess, P.R.C. Kent, J.B. White, *Phys. Rev. Lett.* **95**, 237001 (2005)
 - ¹⁸ P. Sahebsara and D. Sénéchal, *Phys. Rev. Lett.* **97**, 257004 (2006).
 - ¹⁹ B. Kyung and A. M. S. Tremblay, *Phys. Rev. Lett.* **97**, 046402 (2006).
 - ²⁰ H. Yokoyama, M. Ogata, and Y. Tanaka, *J. Phys. Soc. Jpn.* **75**, 114706 (2006).
 - ²¹ T. Mizusaki and M. Imada, *Phys. Rev. B* **74**, 014421 (2006).
 - ²² E. Shender, *Sov. Phys. JETP* **56**, 178 (1982).
 - ²³ P. Chandra and B. Doucot, *Phys. Rev. B* **38**, 9335 (1988).
 - ²⁴ For a review see G. Misguich and C. Lhuillier, cond-mat/0310405 (2003).
 - ²⁵ A. Auerbach, *Interacting electrons and quantum magnetism* (Springer-Verlag New York, 1994), chap. 3.
 - ²⁶ J.-Y. P. Delannoy, M. J. P. Gingras, P. C. W. Holdsworth, and A.-M. S. Tremblay, unpublished.
 - ²⁷ J. Y. P. Delannoy, M. J. P. Gingras, P. C. W. Holdsworth, and A. M. S. Tremblay, *Phys. Rev. B* **72**, 115114 (2005).
 - ²⁸ T. Maier, M. Jarrell, T. Pruschke, and M. H. Hettler, *Rev. Mod. Phys.* **77**, 1027 (2005).
 - ²⁹ A. M. S. Tremblay, B. Kyung, and D. Senechal, *Low Temp. Phys.* **32**, 424 (2006).
 - ³⁰ M. Potthoff, *Eur. Phys. J. B* **32**, 429 (2003).
 - ³¹ M. Potthoff, *Eur. Phys. J. B* **36**, 335 (2003).
 - ³² M. Aichhorn, E. Arrighoni, M. Potthoff, and W. Hanke, *Phys. Rev. B* **74**, 024508 (2006).
 - ³³ R. Freund, *Band Lanczos method*. In *Templates for the Solution of Algebraic Eigenvalue Problems: A Practical Guide*, edited by Z. Bai, J. Demmel, J. Dongarra, A. Ruhe, and H. van der Vorst (SIAM, Philadelphia, 2000).
 - ³⁴ M. Aichhorn, E. Arrighoni, M. Potthoff, and W. Hanke, cond-mat/0607271 (2006).
 - ³⁵ S. R. Hassan, B. Davoudi, B. Kyung, and A.-M. S. Tremblay (unpublished).
 - ³⁶ W. H. Press *et al.*, *Numerical recipes in C++: the art of scientific computing* (Cambridge Univ. Press, 2002), chap. 10.
 - ³⁷ W. Hofstetter and D. Vollhardt, *Ann. Physik* **7**, 48 (1998).
 - ³⁸ M. Imada and T. Kashima, *J. Phys. Soc. Jpn.* **69**, 2723 (2000); T. Kashima and M. Imada, *ibid.* **70**, 2287 (2001).
 - ³⁹ H. J. Schulz and T. A. L. Ziman, *Europhys. Lett.* **18**, 355 (1992); T. Einarsson and H. J. Schulz, *Phys. Rev. B* **51**, 6151 (1995).
 - ⁴⁰ O. Parcollet and G. Biroli, and G. Kotliar, *Phys. Rev. Lett.* **92**, 226402 (2004).
 - ⁴¹ A. Damascelli, Z. Hussain, and Z.-X. Shen, *Rev. Mod. Phys.* **75**, 473 (2003).
 - ⁴² B. Kyung, private communication.
 - ⁴³ B. Kyung, *Phys. Rev. B* **75**, 033102 (2007).
 - ⁴⁴ M. Vekić and S. R. White, *Phys. Rev. B* **47**, 1160 (1993).
 - ⁴⁵ T. Senthil, A. Vishwanath, L. Balents, S. Sachdev, M.P.A. Fisher, *Science* **303**, 1490 (2004); T. Senthil, Leon Balents, Subir Sachdev, Ashvin Vishwanath, and Matthew P. A. Fisher, *Phys. Rev. B* **70**, 144407 (2004)